International Journal of
Advances in Scientific Research and Engineering (ijasre)

E-ISSN : 2454-8006

DOI: http://dx.doi.org/10.7324/IJASRE.2017.32494

Vol.3 (8) Sep - 2017

Multipath Interference Reduction In Wireless Radio Systems Using Two-Branch Selection Diversity

Okorafor. C.I[1] Omeje Anene[2] Chukwuneke.N.S[3] and Okorogu V.N[1]

Department of Electronics and Computer Engineering

Faculty of Engineering

Awka, Anambra

Nigeria

ABSTRACT

Fading is a major impairment when transmitting a signal in wireless communication channel. It is caused by multipath propagation. That is signals from different paths can constructively or destructively interfere with each other. Thus, it becomes very necessary to reduce this effect, to transmit the signal effectively to the receiver This work explains the concept of multipath interference as well as technique used in reducing such, which include the two branch selection diversity that analytically derives an upper bound for the output power of two-sensor branch-selection reception, based on an empirically proven "geometric model" of the wireless propagation channel. Diversity techniques are very useful to improve the performance of high speed wireless channel to transmit data and information.

Key Words: *Multipath Interference, Two-Branch Selection Diversity, Upper Bound, Output Power.*

1. INTRODUCTION

Multipath interference is a phenomenon in the physics of waves whereby a wave from a source travels to a detector via two or more paths and, under the right condition; the two (or more) components of the wave interfere. Multipath interference is a common cause of "ghosting" in analog television broadcasts. The condition necessary is that the components of the wave remain coherent throughout the whole extent of their travel. The interference will arise owing to the two (or more) components of the wave having, in general, travelled a different length (as measured by optical path length, geometric length and refraction (differing optical speed)), and thus arriving at the detector out of phase with each other. The signal due to indirect paths interferes with the required signal in amplitude as well as phase which is called multipath fading.

In wireless telecommunications, multipath is the propagation phenomenon that results in radio signals reaching the receiving antenna by two or more paths. Causes of multipath include atmospheric ducting, ionospheric reflection and refraction, and reflection from water bodies and terrestrial objects such as mountains and buildings. The effects of multipath include constructive and destructive interference, and phase shifting of the signal. Destructive interference causes fading. Where the magnitudes of the signals arriving by the various paths have a distribution known as the Rayleigh distribution, this is known as Rayleigh fading. Where one component (often, but not necessarily, a line of sight component) dominates, a Rician distribution provides a more accurate model, and this is known as Rician fading.

Examples of multipath propagation in facsimile and (analog) television transmission, include jitter and ghosting, seen as a faded duplicate image to the right of the main image. Ghosts occur when transmissions bounce off a mountain or

other large object, while also arriving at the antenna by a shorter, direct route, with the receiver picking up two signals separated by a delay. Radar multipath echoes from an actual target cause ghosts to appear.

In radar processing, multipath causes ghost targets to appear, deceiving the radar receiver. These ghosts are particularly bothersome since they move and behave like the normal targets (which they echo), and so the receiver has difficulty in isolating the correct target echo. These problems can be overcome by incorporating a ground map of the radar's surroundings and eliminating all echoes which appear to originate below ground or above a certain height. In digital radio communications (such as GSM) multipath can cause errors and affect the quality of communications. The errors are due to intersymbol interference (ISI). Equalisers are often used to correct the ISI. Alternatively, techniques such as orthogonal frequency division modulation, rake receivers and two-branch selection diversity may be used. In a Global Positioning System receiver, Multipath Effect can cause a stationary receiver's output to indicate as if it were randomly jumping about or creeping. When the unit is moving the jumping or creeping is hidden, but it still degrades the displayed accuracy.

Multipath propagation may also happen in wired media, especially where impedance mismatch causes signal reflection. A well-known example is power line communication. High-speed power line communication systems usually employ multi-carrier modulations to avoid the intersymbol interference that multipath propagation would cause [1].

Mathematical model of the multipath impulse response

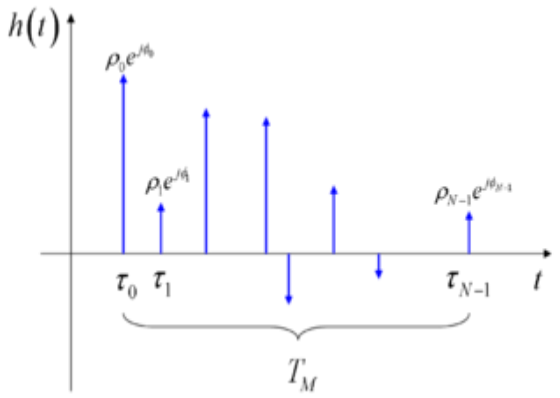

Fig 1.1 Mathematical model of the multipath impulse response.

The mathematical model of the multipath can be presented using the method of the impulse response used for studying linear systems. Suppose you want to transmit a single, ideal Dirac pulse of electromagnetic power at time 0, i.e.

$$x(t) = \delta(t)$$

At the receiver, due to the presence of the multiple electromagnetic paths, more than one pulse will be received (we suppose here that the channel has infinite bandwidth, thus the pulse shape is not modified at all), and each one of them will arrive at different times. In fact, since the electromagnetic signals travel at the speed of light, and since every path has a geometrical length possibly different from that of the other ones, there are different air travelling times (consider that, in free space, the light takes 3 μs to cross a 1 km span). Thus, the received signal will be expressed by

$$y(t) = h(t) = \sum_{n=0}^{N-1} \rho_n e^{j\phi_n} \delta(t - \tau_n)$$

where N is the number of received impulses (equivalent to the number of electromagnetic paths, and possibly very large), τ_n is the time delay of the generic n^{th} impulse, and $\rho_n e^{j\phi_n}$ represent the complex amplitude (i.e., magnitude and phase) of the generic received pulse. As a consequence, $y(t)$ also represents the impulse response function $h(t)$ of the equivalent multipath model[1].

More in general, in presence of time variation of the geometrical reflection conditions, this impulse response is time varying, and as such we have

$$\tau_n = \tau_n(t)$$
$$\rho_n = \rho_n(t)$$
$$\phi_n = \phi_n(t)$$

Very often, just one parameter is used to denote the severity of multipath conditions: it is called the multipath time, T_M, and it is defined as the time delay existing between the first and the last received impulses

$$T_M = \tau_{N-1} - \tau_0$$

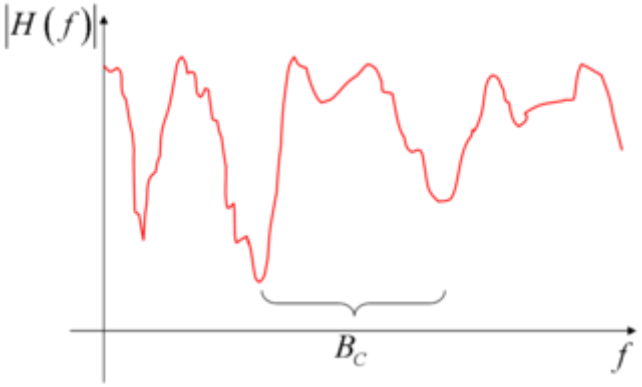

Fig 1.2 Mathematical model of the multipath channel transfer function.

In practical conditions and measurement, the multipath time is computed by considering as last impulse the first one which allows to receive a determined amount of the total transmitted power (scaled by the atmospheric and propagation losses), e.g. 99%.

Keeping our aim at linear, time invariant systems, we can also characterize the multipath phenomenon by the channel transfer function $H(f)$, which is defined as the continuous time Fourier transform of the impulse response $h(t)$

$$H(f) = \mathfrak{F}(h(t)) = \int_{-\infty}^{+\infty} h(t) e^{-j2\pi ft} dt = \sum_{n=0}^{N-1} \rho_n e^{j\phi_n} e^{-j2\pi f\tau_n}$$

where the last right-hand term of the previous equation is easily obtained by remembering that the Fourier transform of a Dirac pulse is a complex exponential function, an eigen function of every linear system. The obtained channel transfer characteristic has a typical appearance of a sequence of peaks and valleys (also called *notches*); it can be shown that, on average, the distance (in Hz) between two consecutive valleys (or two consecutive peaks), is roughly inversely proportional to the multipath time. The so-called coherence bandwidth is thus defined as

$$B_C \approx \frac{1}{T_M}$$

For example, with a multipath time of 3 μs (corresponding to a 1 km of added on-air travel for the last received impulse), there is a coherence bandwidth of about 330 kHz[1].

2. TWO BRANCH SELECTION DIVERSITY TECHNIQUE

Diversity combining is the technique applied to combine the multiple received signals of a diversity reception device into a single improved signal. Diversity combining reduces one possible single-point failure: any single receiver failure, or local interference to a single receiver, will not block reception on the entire system. Equipment sites can

host many radio transmitters and receivers. A single site is subject to local, site-specific interfering signals. These interfering signals may come and go as transmitters switch on and off.

A potential problem with receivers located at high-elevation receiver sites is that they may acquire signals from distant counties, prefectures, or other provinces. These unwanted, distant signals can be stronger than desired signals from local walkie-talkies. The distant signals may block local weak signals in some cases. Having several receive sites increases the probability that one of the sites will receive the local signal in the presence of a distant, undesired one. Selective calling can eliminate users having to listen to the audio of distant signals even though the distant signals are within receive range of one or more receivers [1].

3. THE BRANCH-SELECTION STRATEGY OF SPACE-DIVERSITY WIRELESSRECEPTION

For a wireless receiver equipped with multiple sensors, the receiver may choose among (or may combine) various sensors' individual measurements, to produce an improved composite signal, thereby improving the wireless link's data rate, signal-to-noise ratio, and reliability. "Space diversity" reception (a.k.a. "spatial diversity" reception) refers to the above pre-detection procedure using sensors at distinct locations. The motivation is as follows: Two identical sensors, spaced apart as little as a fractional wavelength, may register signals of widely different amplitudes. This is because each propagation-multipath would undergo its unique sequence of reflections and diffractions, plus corruption by multiplicative noise. When a propagation multipath arrives at a sensor, its aforementioned history would define that propagation multipath's amplitude, Doppler, arrival angle, and arrival time delay. Many such propagation multipaths will sum together, constructively or destructively, to produce the signal measured at that sensor. Whether this summation is constructive or destructive depends critically on the sensor's spatial location. Destructive summation at one sensor needs not preclude a link disconnection, because non-destructive summation could occur at another sensor. "Space diversity" reception often uses as few as two sensors. Standards that use two receive-antennas include: IEEE 802.16e (i.e., WiMAX), IEEE 802.11g and IEEE 802.11n for Wireless LAN. Branch selection" (a.k.a. "antenna selection," "selection diversity," or "selection combining") is one common "space diversity" reception strategy, selecting the sensor (among all sensors) with the strongest reception at a given time moment, for use by the detector. "Branch *selection*" differs from "branch *switching*," which stays with the current sensor so long as its power exceeds a pre-set threshold. "Branch *selection*" is algorithmically simpler than "branch *combining*," which weights and sums all sensors' individual signals. These summation weights would be set as identical in "*equal gain* combining," but would be set to produce coherent summation in "*maximal-ratio* combining." This present work focuses on two-sensor "branch selection" reception. Two-sensor "branch selection" is common in base stations for Wi-Fi networking and for cordless telephones. There, the two antennas are usually spaced apart by about a wavelength[2].

4. CONTRIBUTION OF THE PRESENT WORK

This paper will analytically derive an upper bound of the output power of two-branch selection in wireless space-time reception. The subsequent derivation will employ a specific geometric model, that has been *empirically* verified to produce faithful expressions for the second-order spatial correlation coefficient across two receive-antennas, while coinciding with the well known formula in (1). Section I will define the geometric model of the fading
channel. Section II will derive the mean upper bound, the tightness of which will be accessed via Monte Carlo simulations in Section III.

4.1 The Geometric Model Of The Fading Channel

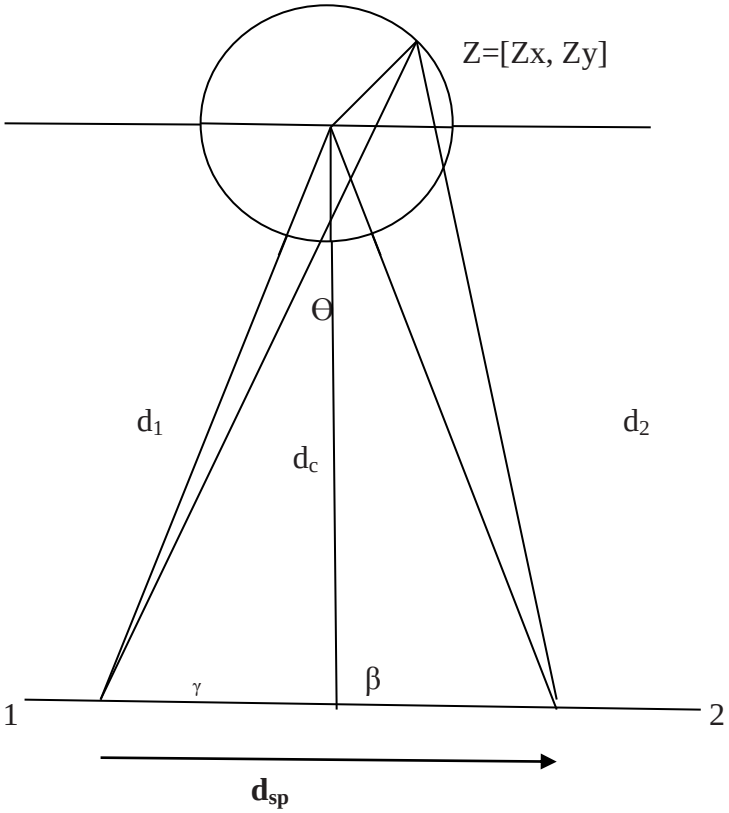

Fig.4.1. The spatial geometry inter-relating the transmitter, the scatterers, and the two sensors of the receiver.

Referring to Fig.4.1, a transmitter is located at $\mathbf{Z}_{Tx}$ = [0, 0] (i.e. centre of the circle) on a two-dimensional Cartesian plane $\mathcal{R}^2$, and emits omnidirectionally. Also on this plane are many scatterers. Here, each scatterer acts as a lossless omnidirectional re-transmitter, producing one multipath towards each sensor. The transmitted signal bounces off every scatterer, in parallel, producing many multipaths towards each sensor of the receiver. That is, if $\mathcal{S}$ number of scatterers exist in $\mathcal{R}^2$, then $\mathcal{S}$ multipaths will travel from the transmitter to *each* sensor, with each multipath representing one "bounce" off a *distinct* scatterer.

A. The Scatterers' Spatial Distribution

The scatterers' locations are modeled as spatially distributed according to a two-dimensional heterogeneous Poisson spatial point process $\Pi(\mathcal{B})$indexed on subsets of $\mathcal{R}^2$. For any $\mathcal{B}$, the random number $\Pi(\mathcal{B})$ of points in$\mathcal{B}$ is distributed according to a Poisson law with parameter $\Lambda(\mathcal{B})$ = $\mathbf{E}[\Pi(\mathcal{B})]$, the expected number of scatterers in the $\mathcal{B}$ set . The scatterer-field itself is

random, with the number and the locations of the scatterers in any $d\mathbf{z} \in \mathcal{R}^2$ randomized, according to the Poisson law with parameter $\Lambda(d\mathbf{z})$. The present model specifies the statistical expectation of the scatterer-field's spatial density, not the spatial density itself. This Poisson model could thus account for the variability in the scatterers' locations, from one field scenario to another. This Poisson field has a heterogeneous intensity, specifically a *uni*-Gaussian (a.k.a. "bivariate Gaussian" in statistics) intensity,

$$\Lambda(d\mathbf{z}) = 1/2\pi\sqrt{\{(1-\rho^2)\sigma_x^2\sigma_y^2\}}$$

$$\exp\{-(z_x^2 + z_y^2 - 2\rho\sigma_x\sigma_y z_x z_y)/2(1-\rho^2)\sigma_x^2\sigma_y^2\}dz \quad \ldots\ldots(1)$$

$$= 1/2\pi|\boldsymbol{\Sigma}|^{1/2} \exp\{-1/2\mathbf{z}^H\boldsymbol{\Sigma}^{-1}\mathbf{z}\}\mathbf{z},$$

where $\boldsymbol{\Sigma} = \begin{vmatrix} \sigma_x^2 & \rho\sigma_x\sigma_y \\ \rho\sigma_x\sigma_y & \sigma_y^2 \end{vmatrix}$

$\mathbf{z} = \begin{vmatrix} z_x \\ z_y \end{vmatrix}$ There, σ_x and σ_y

symbolize the scatterers' root-mean-square spatial spread along the x-axis and the y-axis, respectively. The parameter ρ controls the relationship of the spatial spread between the
two Cartesian axes. The superscript H denotes the Hermitian operator. That which is Gaussian here is the parameter $\Lambda(d\mathbf{z})$[4]. This model (of the scatterers' spatial distribution) has been *empirically* verified to produce faithful expressions for the second-order spatial correlation coefficient across two receive-antennas in wireless multipath fading. In this uni-Gaussian *intensity*, the *expected* number of scatterers decreases, as it gets farther from the transmitter. This mathematical property is physically appealing: For a scatterer closer to the transmitter, that scatterer would less likely be blocked from the transmitter by other scatterers. Hence, the nearer a scatterer is to the transmitter, the more probable that scatterer would be reached by the transmitter and could thus re-transmit towards the sensor. Hence, a scatterer closer to the transmitter would likely have more impact on the overall multipath profile. That is, a scatterer's re-transmission activity depends on that scatterer's spatial location, but it is mathematically simpler to model all scatterers as identical re-transmitters and more densely populated closer to the transmitter.

B. The Re-Transmitted Multipaths' Initial Phases

Consider a multipath bouncing off a scatterer at $\mathbf{z} = [z_x, z_y]$ and reaching sensor

#1 at $\mathbf{z}_{\mathrm{Rx},1} = -(d_1\cos(\beta-\theta),\ d_1\sin(\beta-\theta))$.

This arriving multipath equals the transmitted signal multiplied by the channel-induced complex-valued coefficient

$c_1(\mathbf{z}) = e^{j\varphi(\mathbf{z})}$ ..... (2)

Similarly for a multipath reaching sensor

#2 at $\mathbf{z}_{\mathrm{Rx},2} = (d_{sp}-d_1\cos(\beta-\theta), -d_1\sin(\beta-\theta))$.

$c_2(\mathbf{z}) = e^{j(\varphi(\mathbf{z})-\Delta(\mathbf{z}))}$ ..... (3)

These multipaths share the same initial phase of $(\mathbf{z})$, incurred when they are re-transmitted by the scatterer at $\mathbf{z}$. This initial phase is modeled as uniformly random over $(-\pi, \pi)$, i.e. $[(\mathbf{z})/\mathbf{z}] \sim U(-\pi, \pi)$. This initial phase is also modeled as statistically independent of $\Pi(\mathscr{R}^2)$. This *initial* phase $(\mathbf{z})$ depends on only the scatterer's location, but not the sensor's location. Furthermore, any two scatterers' initial phases are modeled as statistically independent. For the multipaths' temporal phase-difference $\Delta(\mathbf{z})$ between sensors #1 and #2 at the receiver,

$\Delta(\mathbf{z}) = 2\pi/\lambda\ [s_1(\mathbf{z}) - s_2(\mathbf{z})]$.

Referring to the spatial geometry in Fig.4.1,

$[s_\ell(\mathbf{z})]^2 = [a(\mathbf{z})]^2 + d_\ell^2$

$+2(\mathbf{z})_\ell\cos(a(\mathbf{z}) - \gamma\ell(\mathbf{z}_{\mathrm{Tx}})),\quad \forall\ell = 1, 2,$

where $a(\mathbf{z}) = /\mathbf{z} - \mathbf{z}_{\mathrm{Tx}}/$ denotes the distance between the transmitter and the scatterer at z. Hence,

$\Delta(\mathbf{z}) = 2\pi/\lambda\,[\sqrt{d_1^2 + 2a(\mathbf{z})d_1\cos(a(\mathbf{z}) - \gamma 1(\mathbf{z}_{\mathrm{Tx}})) + a(\mathbf{z})^2} - \sqrt{d_2^2 + 2(\mathbf{z})_2\cos(a(\mathbf{z}) - \gamma 2(\mathbf{z}_{\mathrm{Tx}})) + a(\mathbf{z})^2}\,]$

$\simeq 2\pi/\lambda\,[d_1 - d_2 + (\mathbf{z})\,(\zeta_x\cos(\mathbf{z}) - \zeta_y\sin(\mathbf{z}))] = 2\pi/\lambda\,[d_1 - d_2 + \langle\boldsymbol{\zeta}, \mathbf{z} - \mathbf{z}_{\mathrm{Tx}}\rangle]$ .....(4)

where λ symbolizes the wireless signal's carrier-wavelength,

$\boldsymbol{\zeta} = [\zeta_x, -\zeta_y]$, $\zeta_x = 2/(d_1+d_2)[d_{sp}-(d_1-d_2)\cos(\theta)\cos(\beta)]$,

$\zeta_y = 2/(d_1+d_2)(d_1 - d_2)\cos(\theta)\sin(\beta)$, and $\langle \mathbf{v}_1, \mathbf{v}_2 \rangle$

denotes an inner vector-product between two size-compatible vectors $\mathbf{v}_1$ and $\mathbf{v}_2$. The above approximation in (4) holds for $d_c \gg$ trace (Σ) and $d_c \gg d_{sp}$ [3]. These two inequalities, together, require each scatterer to be sufficiently close to the

mobile relative to the basestation. Applicable field scenarios include basestations elevated on a tower or otherwise not immediately surrounded by prominent scatterers[3].

4.2. The Derivation Of A Mean Upper Bound Of The Output Power

The vector-sum of the stochastic fading coefficients of all multipaths that arrive at sensor #1 gives sensor #1's fading-gain,

$C_1 = \int_{\mathbb{R}2} c_1(z)\Pi(dz) = \int_{\mathbb{R}2} e^{j\varphi(z)}\Pi(dz)$, ... (5)

with $E_{\Pi, z, \varphi}\{C1\} = \int_{\mathbb{R}2} E\{e^{j\varphi(z)}\}\{\Pi(dz)\} = 0$.

Analogously, sensor #2's fading-gain equals

$C_2 = \int_{\mathbb{R}2} c_2(z)\Pi(dz) = \int_{\mathbb{R}2} e^{j(\varphi(z)-\Delta(z))}\Pi(dz)$..... (6)

Two-sensor branch-selection reception's output power equals **(**max $\{/C_1/^2, /C_2/^2\}$**).**Here, C_1, C_2, and **(**max $\{/C_1/^2, /C_2/^2\}$**)**are stochastic variables, dependent on Π, **z**, and φ. To obtain the *expected* output power, apply the "Law of Total Expectation":

$E_{\Pi, z, \varphi}(\max\{/C_1/^2, /C_2/^2\}) = E_{\Pi, z}[E_{\varphi}(\max\{/C_1/^2, /C_2/^2\}) / \Pi, z)]$..... (7)

The above expectation is taken first with regard to φ, in order to ease the subsequent derivation. For any specific realization of Π, the number of scatterers is set, and (5) and (6) would have their integrals become finite sums, which are easier to manipulate. For the inner expectation in (7), derivation for the upper bound is as follows:

$E_{\varphi}(\max\{/C_1/^2, /C_2/^2\}) / \Pi = n, z_1, \ldots z_n)$

$\leq n + 4/\sum_{(i=2 \text{ to } n)}\sum_{(l=1 \text{ to } i-1)}\{\text{Sin}\delta_{i,l}/2\}$, ... (8)

with $\delta_{i,l} = \Delta(z_i) - \Delta(z_l) = 2\pi/\lambda(\zeta, z_i - z_l)$

being a random variable $\forall i, l$, is dependent on Π and **z**, but not on φ. The equality holds in (8) at Π = 1 and Π = 2, for any Poisson intensity. The *in*equality in (8) holds for any Poisson intensity,
not only for the uni-Gaussian intensity defined in Section II-A. If the Poisson process has the uni-Gaussian intensity of (1) in Section II, the following mean upper bound of the two-sensor branch-selection reception output is:

$E_{\Pi, z, \varphi}[\max\{/C_1/^2, /C_2/^2\}]$

$\leq (s^2) = 1 + 2/\pi e^{-s^2/2}\{\text{Erfi}[\sqrt{(s^2/2)}]\} + \sum_{(k=1 \text{ to } \infty)} 2(-1)^{k-1}\text{Imag}\{\text{Erf}(k\pi - js^2/(\sqrt{2}s^2)\}$..... .....(9)

$\leq (s^2) = 1 + 2/\pi e^{-s^2/2}[\text{Erfi}(\sqrt{(s^2/2)} + \sum_{(k=1 \text{ to } K-1)} 2(-1)^{k-1}\text{Imag}\{\text{Erf}(k\pi - js^2/(\sqrt{2}s^2)\} + (-1)^{K-1}$

$\text{Imag}\{\text{Erf}(k\pi - js^2/(\sqrt{2}s^2)\} + 4/\pi\,\Phi(-(K\pi)/s), \quad K = 0, 1, 2, \ldots$ (10)

where $s^2 = (\pi/\lambda)^2(2\zeta_x^2\sigma_x^2 + 2\zeta_y^2\sigma_y^2 - 4\rho\zeta_x\zeta_y\sigma_x\sigma_y)$,.....(11)

with $\text{Erf}(z) = 2/\sqrt{\pi}\int_{(0 \text{ to } z)} e^{-t^2}dt$

$\text{Erfi}(z) = \text{Erf}(jz)/j$

$4/\pi\Phi(-K\pi/s)$,

Hence,

$s^2 \approx 2[\pi(\sigma_x d_{sp})/(d_1\lambda)]^2(\text{Sin}^2\beta)[1 - \rho\text{Sin}(2\beta)]$

for $d_1 \gg d_{sp}$.....(12)

Moreover, the wider the scatterers' are spatially spread, the shorter will this d_{sp} λ threshold be. This is intuitively reasonable:
The smaller d_{sp} or σ_x/d_1 is, more will the scatterers become effectively spatially concentrated, less will be the phase-difference between the two sensors, and thus closer to one (i.e. less) will be the expected output power[8].

4.3. The Tightness Of The Mean Upper Bound Derived In (9)

Monte Carlo simulations of max $\{/C_1/^2, /C_2/^2\}$ (which involves three random entities Π, $\mathbf{z}$, φ) will demonstrate the tightness of its mean upper bound of (10).

A. Monte Carlo Simulation Approach Using the Bernoulli Approximation & Using Importance Sampling
The Monte Carlo simulations are conducted as follows:

(i) The spatial support region will cover $[-3\sigma_x, \ 3\sigma_x] \times [-3\sigma_y, \ 3\sigma_y]$, centered at the point $\mathbf{z}_{Tx}$ on the *x-y* Cartesian plane. This support region will encompass over 99% of all scatterers, given the uni-Gaussian density in Section II-A. Partition this above finite region into $3600\sigma_x\sigma_y$ number of grid subregions, each with area equal to 0.01.
(ii) To lighten the computational load, approximate the Poisson process Π, on a grid over its support region, by Bernoulli trials. This is a common technique in numerical analysis, with this underlying justification: For a sufficiently small grid subregion $d\mathbf{z}$, the Poisson process Π would almost always allow at most one scatterer therein. That sufficiently small sub-region would most *un*likely contain two or more scatterers. Hence, $\Pi(d\mathbf{z})$behaves approximately as a Bernoulli random variable, with probability

$p = (\Pi(d\mathbf{z}) = 1) = \Lambda(d\mathbf{z})e^{-\Lambda(d\mathbf{z})}$..... (13)

Hence, for each grid subregion, the Monte Carlo simulation will realize the random variable $\Pi(d\mathbf{z})$as Bernoulli(p).
(iii) To further lighten the computational load, use "importance sampling" because the $\Pi(d\mathbf{z})$of (13) would produce mostly zeros, as $p \approx 0$ in each region $d\mathbf{z}$. That is, *direct simple* sampling (of the scatterers' Poisson density from the sufficiently small region $d\mathbf{z}$**)** would lead to rare events. However, the variance of rare-event probabilities can be significantly
reduced by applying "importance sampling" instead of "direct sampling." The random variable $\Pi(d\mathbf{z})$is realized from Bernoulli(κp). Here, κ = 30 represents a good value to compromise between simulation accuracy and computation load[9].
(iv) Sum all grid subregions' values of $^{(\mathbf{z})}\Pi(d\mathbf{z})$,to evaluate C_1. Similarly, sum all grid subregions' values of$^{(\varphi(\mathbf{z})-\Delta(\mathbf{z}))}$ $\Pi(d\mathbf{z})$, to evaluate C_2. Compute the maximum between
$/C_1/^2$, *and* $/C_2/^2$, for this one realization.

(v) Each loop through steps (i) to (iv) constitutes one Monte Carlo sampling trial. Lastly, $_{\Pi,\mathbf{z},\varphi}$ max$\{/C_1/^2, /C_2/^2\}$ is approximated by the algebraic average of the values of $1/\kappa$ max$\{/C_1/^2, \ /C_2/^2\}$ obtained from 200 independent Monte Carlo sampling trials[7].

Table.4.1. Monte Carlo Simulation Results

FIG.	β	ρ	σ_x/λ	d_1/λ				d_{sp}/λ
4	60^0	0	12	100,	300,	500,	1000	¼, ½, 2, 10
5	60^0	0	24	100,	300,	500,	1000	¼, ½, 2, 10
6	60^0	½	12	100,	300,	500,	1000	¼, ½, 2, 10
7	30^0	0	12	100,	300,	500,	1000	¼, ½, 2, 10
-	-	-	-	-				-

For each scenario, M = 100 replications of (i) - (v) are performed. The mth replication evaluates the average (denoted as e_m) of the 200 independent Monte Carlo sampling trial values of $\max\{|C_1|^2, |C_2|^2\}$.

This *mean* upper bound can under-estimate, because it is not an *absolute* upper bound, i.e. not absolute over all realizations of the random entities of Π, $\mathbf{z}$, φ [10].

5. CONCLUSION

Analytically derived for the first time in the open literature is an upper bound of the mean output power of a two-sensor branch-selection receiver, based on a geometric model of the fading channel. This expression is explicitly in terms of the channel model's three degrees-of-freedom (namely, β, ρ, and σ_x / d_1) . Monte Carlo simulations verify that the derived mean output power to be accurate to within a very few percentages.

REFERENCES

1. [1] D.G. Brennan, "*Linear diversity combining techniques*," Proc. IRE, vol.47, no.1, pp.1075–1102, June 1959
2. [2] F. Adachi, M. T. Feeney, A. G. Williamson, and J. D. Parsons, "*Cross-correlation between the envelopes of 900 MHz signals received at a mobile radio base station site*," *IEE Proc. Radar Signal Process.*, vol. 133, part F, no. 6, pp. 506–512, Oct. 1986.
3. [3] J. Fuhl, A. F. Molisch, and E. Bonek, "*Unified channel model for mobile radio systems with smart antennas*," *IEE Proc.: Radar, Sonar*
4. *Navigation*, vol. 145, no. 1, pp. 32–41, Feb. 1998.

5. [4] T.-A. Chen, M. P. Fitz, W.-Y. Kuo, M. D. Zoltowski, and J. H. Grimm, "*A space-time model for frequency nonselective Rayleigh fading channels with applications to space-time modems*," *IEEE J. Sel. Areas Commun.*, vol. 18, no. 7, pp. 1175–1190, July 2000.

6. [5] R. Janaswamy, "*Angle and time of arrival statistics for the Gaussian scatter density model*," *IEEE Trans. Wireless Commun.*, vol. 1, no. 3,
7. pp. 488–497, July 2002.

8. [6] C. P. Robert and G. Casella, "*Monte Carlo Statistical Methods"*, 2nd edition. Springer-Verlag, 2004.

9. [7] A. Baddeley and R. Turner, "*Spatstat: an R package for analyzing spatial point patterns*," *J. Statistical Software*, vol. 12, no. 6, pp. 1–42, Jan. 2005.

10. [8] V. I. Piterbarg and K. T. Wong, "*Spatial-correlation-coefficient at the basestation, in closed-form explicit analytic expression, due to heterogeneously Poisson distributed scatterers*," *IEEE Antennas Wireless Propag. Lett.*, vol. 4, pp. 385–388, 2005.

11. [9] A. Doucet and X. Wang, "*Monte Carlo methods for signal processing: a review in the statistical signal processing context*," *IEEE Signal Process. Mag.*, vol. 22, no. 6, pp. 152–170, Nov. 2005.

12. [10] H. Rafati and B. Razavi, "*A receiver architecture for dual-antenna systems*," *IEEE J. Solid-State Circuits*, vol. 42, no. 6, pp. 1291–1999,
13. June 2007.